J. Ocean Univ. China (Oceanic and Coastal Sea Research)
DOI 10.1007/s11802-017-3406-5
ISSN 1672-5182, 2017 16 (4): 674-682
http://www.ouc.edu.cn/xbywb/
E-mail:xbywb@ouc.edu.cn

Swells of the East China Sea

TAO Aifeng[1), 2)], YAN Jin[2)], PEI Ye[3)], ZHENG Jinhai[1), 2), *], and MORI Nobuhito[4)]

1) *Key Laboratory of Coastal Disaster and Defence (Hohai University)*, *Ministry of Education*, *Nanjing* 210098, *P. R. China*
2) *College of Harbor*, *Coastal and Offshore Engineering*, *Hohai University*, *Nanjing* 210098, *P. R. China*
3) *Xiangshui Yangtze Wind Power Generation Co.*, *Ltd*, *Xiangshui* 224600, *P. R. China*
4) *Disaster Prevention Research Institute*, *Kyoto University*, *Gokasho*, *Uji*, *Kyoto* 611-0011, *Japan*

(Received January 3, 2017; revised May 3, 2017; accepted May 17, 2017)

Abstract Over the past few decades, an increasing number of marine activities have been conducted in the East China Sea, including the construction of various marine structures and the passage of large ships. Marine safety issues are paramount and are becoming more important with respect to the likely increase in size of ocean waves in relation to global climate change and associated typhoons. In addition, swells also can be very dangerous because they induce the resonance of floating structures, including ships. This study focuses on an investigation of swells in the East China Sea and uses hindcast data for waves over the past 5 years in a numerical model, WAVEWATCH III (WW3), together with historical climate data. The numerical calculation domain covers the entire North West Pacific. Next, swells are separated and analyzed using simulated wave fields, and both the characteristics and generation mechanisms of swells are investigated.

Key words swell; East China Ocean; numerical simulation

1 Introduction

Swell refers to waves remaining on the sea after the sea wind has abated, weakened, or steered; however, swell can also originate from other waters. In comparison with wind sea, swell has a regular shape with a large wave period, a longer crest line, and a smooth wave surface. The amplitudes of heave and pitch are easily magnified by swell; therefore, floating structures (such as ships and floating platforms) are at risk of damage when encountering swell, even though the actual wave height may be lower than that of wind sea. Sometimes the resonance of floating structures can be induced by swell.

Future wave changes occurring in relation to climate change have been investigated during the last decade (Hemer *et al.*, 2013), and results show a decreasing wave height tendency over the Western North Pacific because of global warming (Shimura *et al.*, 2016). In addition, Shimura *et al.* (2013) showed that wave height climate responses to teleconnection patterns in the eastern part of the North Pacific and North Atlantic are more sensitive than those in corresponding western parts. Swell shows its probability to be component of rogue wave according to recent research. Wang *et al*. (2014) investigated rogue waves off Jiangsu coast by analysis of wave elevation data at Xiangshui buoy, and occurrence possibility of rogue waves was revealed to be random in any wave field (Tao *et al*., 2014). The potential threat of rogue waves against China coastal region points out the importance of swell study. However, studies on the Western North Pacific swell are scarce, even though its importance is attracting increasing attention. Marine shipping is well-developed in the East China Sea, and a large number of marine projects have been established. Marine engineering is often affected by swell during construction and operation processes. There are limited studies focusing on swell; therefore, it is necessary to investigate its influence on marine navigation safety and the development and utilization of marine resources, with the aim of preventing and reducing associated disasters.

The East China Sea lies within the East Asian monsoon region of the Northwest Pacific. It is affected by the monsoon throughout the entire year, and in summer and winter it is subjected to typhoons, cold waves, and other extreme weather. Pei *et al*. (2016) indicated that a region within the East China Sea named E3 affected by swell generated in Northwest Pacific during typhoon scenarios. The effects of these different meteorological conditions on the generation mechanisms and evolutionary characteristics of swells in the East China Sea are considered in this study. In addition, it has been observed that swell can spread from the North Pacific to the northern part of Indian Ocean along a latitude of 30 degrees (approximately 14422.2 km) with little loss of energy (Munk and Snod-

* Corresponding author. Tel: 0086-25-83787706
E-mail: jhzheng@hhu.edu.cn

grass, 1957). Furthermore, swell in the East China Sea can be induced by local winds and propagate from the east side of the Ryukyu chain. Ryukyu chain was proved that has blocking effect on swells caused by ideal wind field originate from the Northwest Pacific (Zhang *et al.*, 1988). In this respect, the influences of different spatial scales used in calculations are considered to clarify the generation mechanisms of swell in the East China Sea. A numerical wave model of the East China Sea based on WAVEWATCHIII is established and validated, and results are analyzed to determine both the characteristics as well as generation mechanisms of swell.

2. Data and Methodology

2.1 Model Setup

The official version 3.14 of WAVEWATCH III is used here (Tolman, 2009). Water depths are derived from the National Geophysical Data Center ETOPO 1 data (Amante and Eakins, 2009), and the resolution is 1/60°×1/60°. Wind field data are derived from CCMP/NCEP & Myers (Liu *et al.*, 2011; Milliff *et al.*, 2004; Myers, 1954) datasets, which are regularly gridded using a 6-hour interval at a resolution of 0.25°×0.25°. Typhoon data are derived from CMABST datasets (Ying *et al.*, 2014).

The model grid is regular in latitude and longitude with a resolution of 0.25°×0.25°, and source terms for energy spectra in the model are set to default. The spectral grid uses 24 directions regularly spaced over a full circle with a directional resolution of 15°, and 24 frequencies from 0.04118 Hz to 0.40561 Hz that are exponentially spaced with a factor increment of 1.1. All parameters, including significant wave height (SWH), spectrum peak period (SPP), and mean wave direction, are extracted from dimensional spectrum for both wind waves and swells.

Based on the WW3 model, two calculation domains are considered within the Northwest Pacific, as shown in Fig.1: D1 (0°–50°N, 100°–160°E) and D2 (24°–41°N, 117°–131°E). These two spatial scales are selected for analyzing the sources of swells in the East China Sea. The time duration of hindcast is from January 1, 2010 to December 31, 2014. All scenarios, including typhoon and monsoon climates, are realized in both D1 and D2 using the same spatial resolution of 0.25°×0.25° and a time step of 3600 s. Simulation results are output each 10800 s in this issue.

2.2 Model Verification

As mentioned above, the source terms of the model are set to default. Therefore, it is necessary to verify the feasibility of the numerical wave model before running numerical realizations (Hanson *et al.*, 2009), and it is more reasonable to verify the feasibility of swell simulation directly using a comparison between numerical results and observed data. However, it is difficult to obtain only the observed data of swells because most available data refer to combined waves; therefore the observed wave data used here for model verification are also those of combined wave data. Version 3.14 of WW3 had been verified in a previous study (Tracy *et al.*, 2007) for its ability to capture swell and to separate wind waves from swells.

The physical parameters of both the significant wave height and the spectrum peak period are used to verify the wave model established over the entire Northwest Pacific Ocean, based on the observed data obtained from two stations: Xiangshui, which is located near Xiangshui in Jiangsu Province, China and Ikitsuki, which is situated near Ikitsuki Island, Japan (Fig.2). The duration of simulations and related climate are shown in Table 1.

A comparison of the simulated values and measured data is shown in Fig.3, where it is evident that simulation results in terms of time-varying patterns are in fairly good agreement with observations at both stations.

The correlation coefficient, bias, mean absolute error, and root mean square error between the simulated and measured values are calculated to quantify the comparison results and are shown in Table 2. The correlation coefficients (CC) are all larger than 0.8, which indicates a

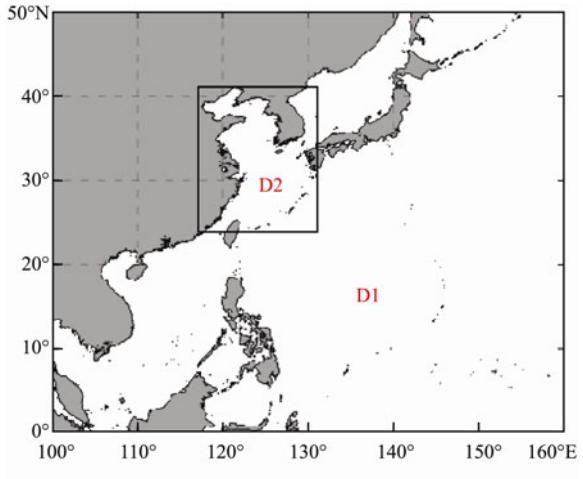

Fig.1 Numerical calculation domains; D1 is the larger domain and D2 the smaller domain.

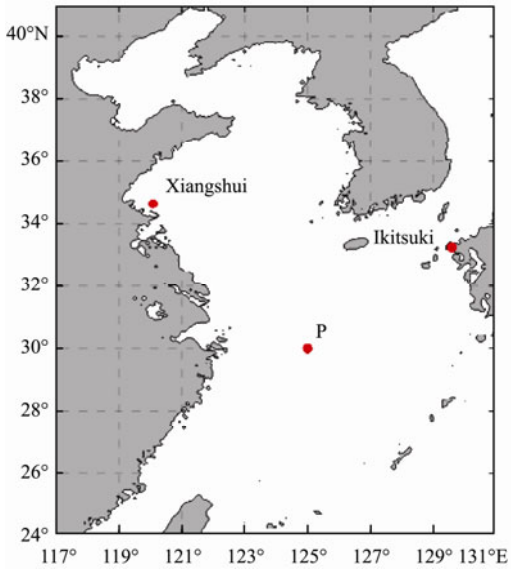

Fig.2 Locations of observation stations and point P.

Table 1 Information pertaining to both observation stations

Station	Observed data duration	Location	Mean water depth (m)	Related climate
Xiangshui	2011.01.01–2011.01.31	120°6′E, 34°26.2′N	8.4	Regular
Ikitsuki	2012.08.10–2012.10.09	129°25.8′E, 33°26.4′N	91	Typhoon & regular

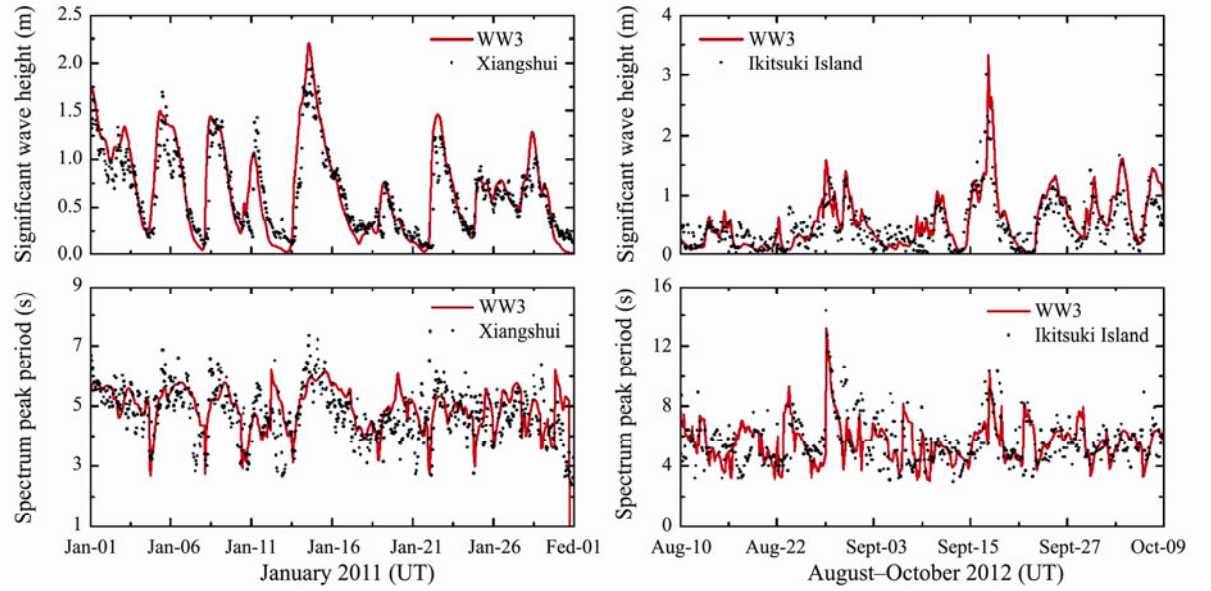

Fig.3 Comparison between measured data and simulated values. Observations and simulations are represented by scatter and line, respectively, over time.

satisfactory correlation between the simulated and measured values. Calculation results of the bias show that the results of both stations are positive but the values are relatively small, indicating that the simulated value of WW3 is slightly larger than the measured value. Both values of the mean absolute error (MAE) and root mean square error (RMSE) are also relatively small and are in the allowable range of the specification. In summary, it is considered that the simulation results of the model are in good accordance with observations, and that the WW3 wave model can be used to simulate wave fields in the East China Sea.

Table 2 Statistical results of comparison between measured data and simulated values

Buoy stations		Statistical parameters			
		CC	Bias	MAE	RMSE
Xiangshui	SWH	0.96	0.05	0.79	0.58
	SPP	0.92	0.38	0.87	0.63
Ikitsuki	SWH	0.85	0.02	0.45	0.49
	SPP	0.82	0.06	0.57	0.61

2.3 Swell Separation

A wave-age criterion is used to identify wind seas, with wind-sea peak lying within the parabolic boundaries defined by (Hanson and Phillips, 2001) the following equation:

$$C_p \le (1.5)U_{10}\cos\delta\,, \tag{1}$$

where C_p is the phase speed of the wind sea, U_{10} is the 10-m elevation wind speed, and δ is the angle between the wind and the wind sea. For the peak frequency of the wind-sea peak in deep water, the equation above becomes

$$f_p \ge \frac{g}{2\pi}(1.5U_{10}\cos\delta)^{-1}, 0\le\delta\le 2\pi\,. \tag{2}$$

A generous factor of 1.5 ensures that all possible wind-sea peaks are included.

3 Analysis of Results

3.1 Spatial and Temporal Distribution of Swell in East China Sea

3.1.1 Temporal distribution of swell in East China Sea

To understand the maximum significant wave heights and correlative spatial distribution of swell possible, we here use the sea state (WMO Sea State) to depict swells in the East China Sea. A representative point labeled ‘P’ (125°E, 30°N) is shown in Fig.2 and is selected to analyze the evolution of swell on a time scale. The time scale of the simulation data chosen for analysis is that of the entire year of 2011.

To illustrate the effects of extreme climate on swells, the evolutionary processes for waves during typhoon ‘Muifa’ are shown in Fig.4. It is evident that when the typhoon moved close to D2 (from July 29 to August 4), the swell dominated at the P-point with a significant wave height of approximately 1 m, and the spectrum peak periods of the swell were mainly distributed at 9–14 s. As the typhoon gradually approached P-point, its effect on the East China Sea also increased. From August 4 to August 8, the waves at P-point were related to wind sea

without swell; however, after the typhoon had moved away from P-point, the swell continued to become a part of mixed waves.

The swells at P-point are computed to determine monthly, quarterly, and annual averages, with the aim of illustrating temporal distribution characteristics. The monthly averaged significant wave heights of swells are mainly less than 1.2 m, with higher values in February, July, and August than other months. The monthly average spectrum peak periods of swells, which seldom reach 12 s, are larger in February, September, and December. The swells in the third quarter are the highest, and the quarterly average significant wave heights of swells are mainly less than 1.0 m and the quarterly average spectrum peak periods of swells are mainly less than 10 s.

The annual-averaged values from 2010 to 2014 are also investigated to determine the inter-annual variability of swells in the East China Sea. The annual-averaged significant wave heights are mainly distributed between 0–1.0 m, and the annual average spectrum peak periods of swells are mainly distributed in 0–10 s. In comparison, the temporal distribution of swells in different years is similar and differences are small.

To gain a quantitative understanding of the distribution of swell under different weather conditions, statistical analysis of swell frequency are presented below. During non-typhoon scenarios, the significant wave heights of swells in the East China Sea are mainly distributed in the interval of 0.1–1.25 m (in Fig.5), and the interval with the largest possibility of occurrence is 0.1–0.5 m and their proportion of occurrence is 54.0%. As with the non-typhoon scenarios, the significant wave heights are mainly distributed in the interval of 0.1–4.0 m during typhoon seasons; however, the interval with the largest possibility of occurrence is 0.5–1.25 m, which occurs at a proportion of 49.5%.

Spectrum peak periods, as shown in Fig.5, are mainly distributed in the 4–15 s section during non-typhoon scenarios; the interval with the largest possibility of occurrence is 8–15 s, at a proportion of 22%. In addition, dur-

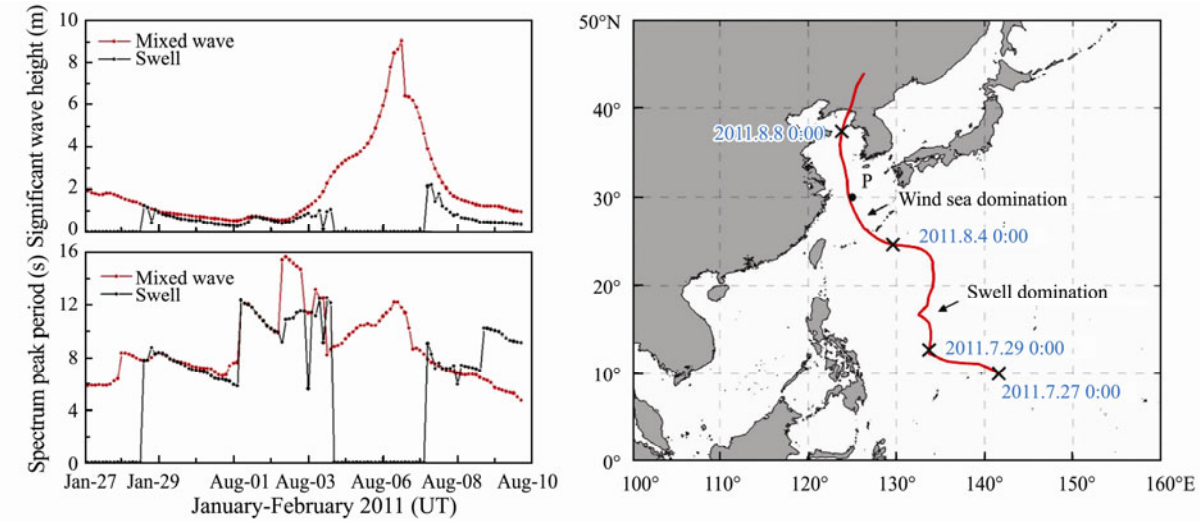

Fig.4 Comparison between mixed-wave and swell at P-point and movement path of typhoon 'Muifa'. Mixed waves and swell at P-point are identified using red and black, respectively.

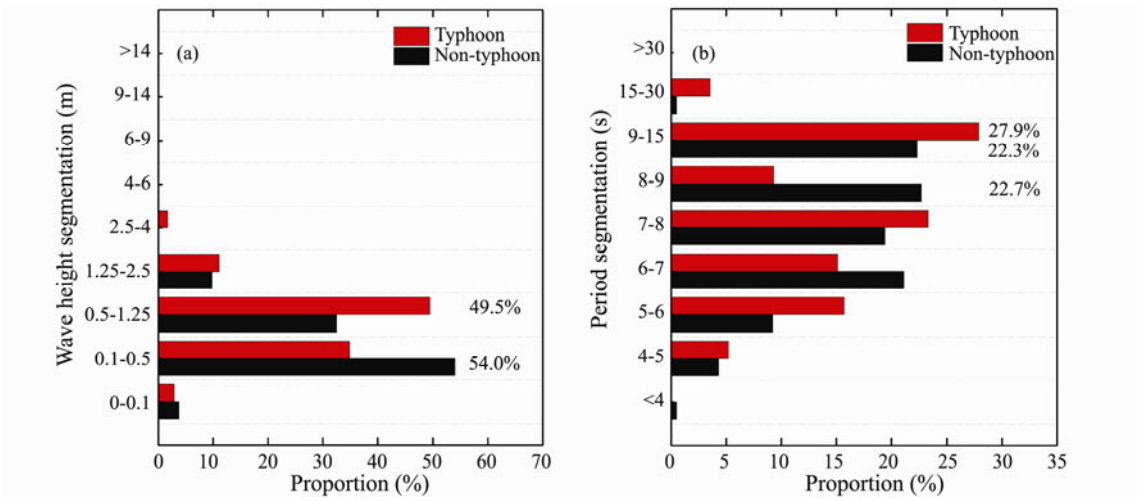

Fig.5. Percentage proportion of occurrence of each sea state during typhoon and non-typhoon scenarios throughout 2010: (a) significant wave height; (b) spectrum peak period.

ing typhoon scenarios, the spectrum peak periods are mainly distributed in the interval of 4–30 s; the interval with the largest possibility of occurrence is 8–15 s, at a proportion of 27.9%.

The proportion of time that each sea state occurred during 2010–2014 is then computed to reveal the annual variation in swell, as shown in Fig.6. The main properties of the distribution ranges are consistent, although corresponding frequencies are not exactly identical. Significant wave heights of swells in the East China Sea are mainly distributed between 0.1 m and 2.5 m, with a largest possibility interval of 0.1–0.5 m, at an annual frequency of 49%. The distribution range of spectrum peak periods is 4–15 s, and the maximum possible interval is 9–15 s.

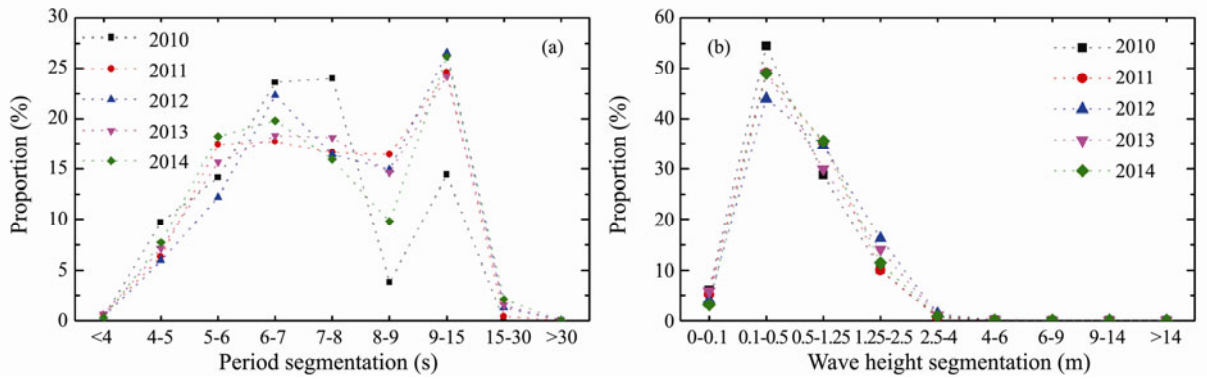

Fig.6 Percentage proportion of occurrence of each sea state during 2010–2014: (a) spectrum peak period, (b) significant wave height.

3.1.2 Spatial distribution of swells in East China Sea

Swell data from 2011 are used as an example to illustrate the spatial distribution of swells. The sea state produced by swell in some of the offshore sea areas is referred to as Code 1 (0–0.1 m) (in Fig.7), whereas that occurring in most sea areas is referred to as Code 2 (0.1–0.5 m), and that occurring in areas outside the Ryukyu Islands is referred to as Code 3 (0.5–1.25 m). Swells within the East China Sea varied in the range of 0.1–0.5 m, which suggests that the energy of swells in the East China Sea is relatively lower than that in the Northwest Pacific. In addition, swells in the sea outside the Ryukyu chain are significantly higher than that inside the chain, which indicates there is a blocking effect from the chain. It also can be seen from Fig.7 that the spatial distribution characteristics of significant wave heights of swells for the simulated 5 years are almost constant. Therefore, this suggests that, at least from a statistical perspective, the spatial distribution characteristics of significant wave heights of swells are mainly related to the effect of topography; this will be investigated in detail in another paper.

The maximum likelihood spectrum peak periods of swells in 2011 are also investigated, as shown in Fig.8. Most areas outside the Ryukyu chain, and half of the East China Sea, are labeled as Code 7 (9–15 s). When swells close to the islands belong to the Ryukyu chain their spectrum peak periods have a decreasing trend, particularly on the northwest side of the chain. Compared to areas outside the chain, half of those inside the chain are labeled as Code 7, which means that the swells belonging to these areas have a high possibility of varying in the range of 0–9 s. This period distribution illustrates the increasing trend in the spectrum peak period from offshore to the deep sea and from north to south.

Unlike the significant wave height distribution of swells, there are certain differences in the spectrum peak period distribution. It is evident that swells with Code 5 (7–8 s) dominated most part of the East China Sea in 2010, while swells with Code 7 (9–15 s) dominated in 2011–2014. Furthermore, swells dominating outside the Ryukyu chain in 2010 and 2013 were Code 5, whereas they were Code 7 in 2011, 2012, and 2014.

3.1.3 Relationship between typhoon and swell

A total of 114 typhoons were recorded in the Northwest Pacific Ocean during the simulated 5 years; however, the effect days of the typhoons differ and are thus considered here, as shown in Fig.9. The annual mean significant wave heights of swells at P-point are computed to compare effect days of typhoons and the significant wave height of swells. From Fig.9, it is evident that the value of the significant wave height of swells increases with the number of extreme weather events. Therefore, it is proven that the length of the typhoon effect is positively correlated with the significant wave height of swells. However, there is not simply a linear relation between these two parameters; therefore, many factors, such as the moving path of the typhoon, need to be considered.

3.2 Generation Mechanisms of Swells in East China Sea

The generation mechanisms of swells are analyzed separately for typhoon and non-typhoon scenarios. As mentioned in Section 2, domain D1 and D2 are selected to identify the sources of swells. Simulation results from D1 grid could present swells originate from waters outside

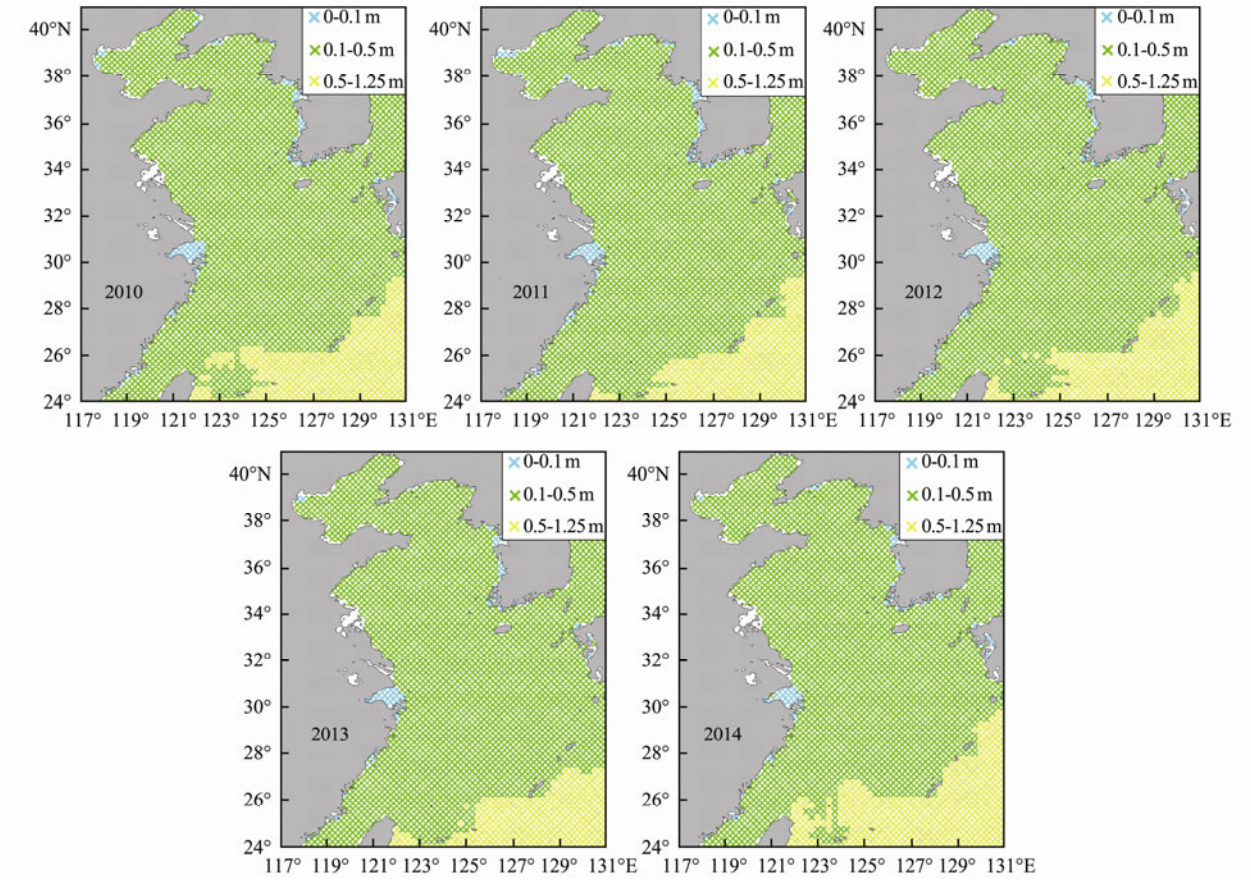

Fig.7 Spatial distribution of maximum significant wave heights of swell during 2010–2014.

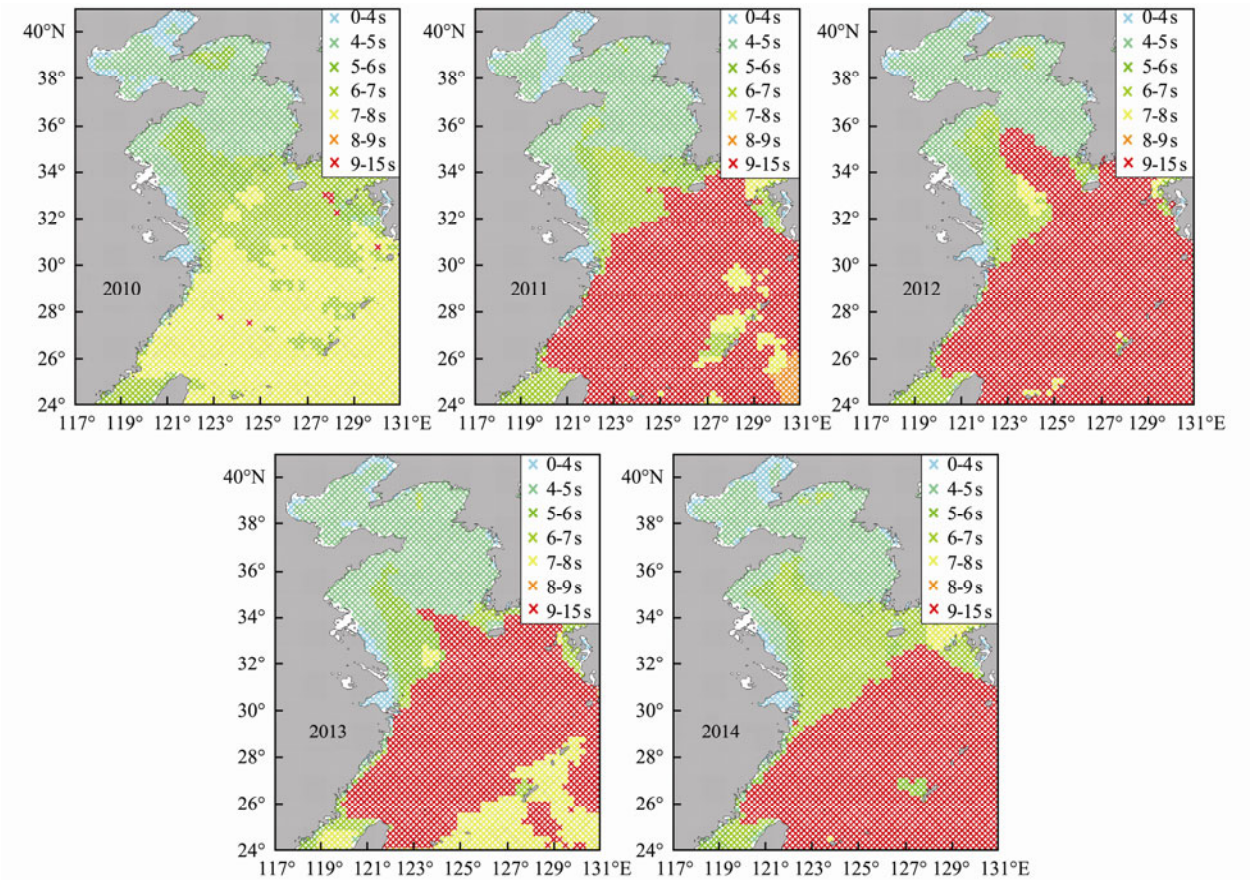

Fig.8 Spatial distribution of maximum likelihood spectrum peak period of swells in 2011.

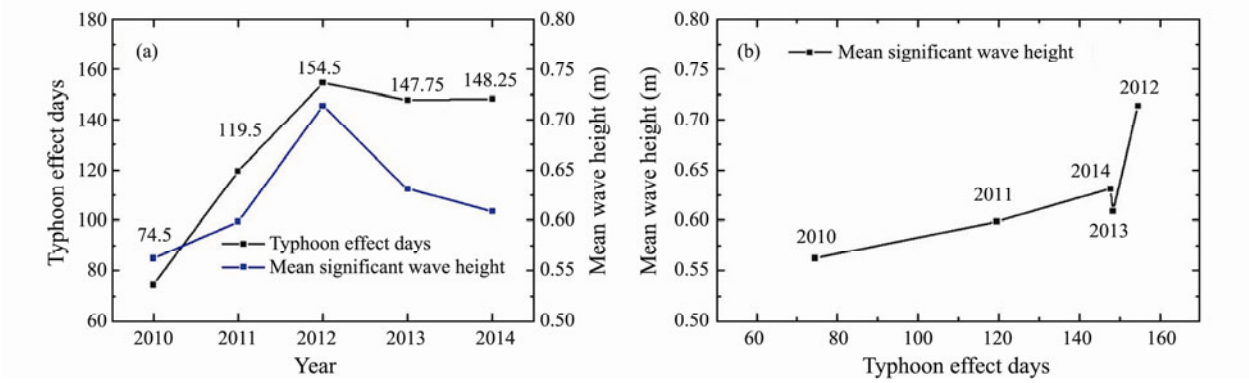

Fig.9 Relationship between typhoon and wave height. (a) Typhoon information from 2010–2014; (b) comparison between effect days of the typhoon and mean wave height of swell at P-point.

and inside the Ryukyu chain, whereas, D2 could only simulate swell generate in the East China Sea. Simulation results for the scales of D1 (Northwest Pacific) and D2 (East China Sea) are compared; from Fig.10 it is evident that four types of comparisons can be made from the results using the various scales. Firstly, results are almost identical for the different scales; this means that swells are generated purely by the local wind on a small calculation scale for D2 and are labeled as 'generated by local wind' hereinafter. Secondly, the large scale values are larger than those of the small-scale (although small-scale values are not zero), which means that a part of swells propagates from outside of D2 (this state is labeled as 'from both areas' hereinafter). Thirdly, large scale values are non-zero values whereas the small-scale values are zero, which suggests that all swells propagate from outside of D2 (this state is labeled as 'from adjacent sea' hereinafter). Finally (and labeled 'no swells'), the values of both scales are zero, which indicates that no swells exist, at least in consideration of the large scale of D1.

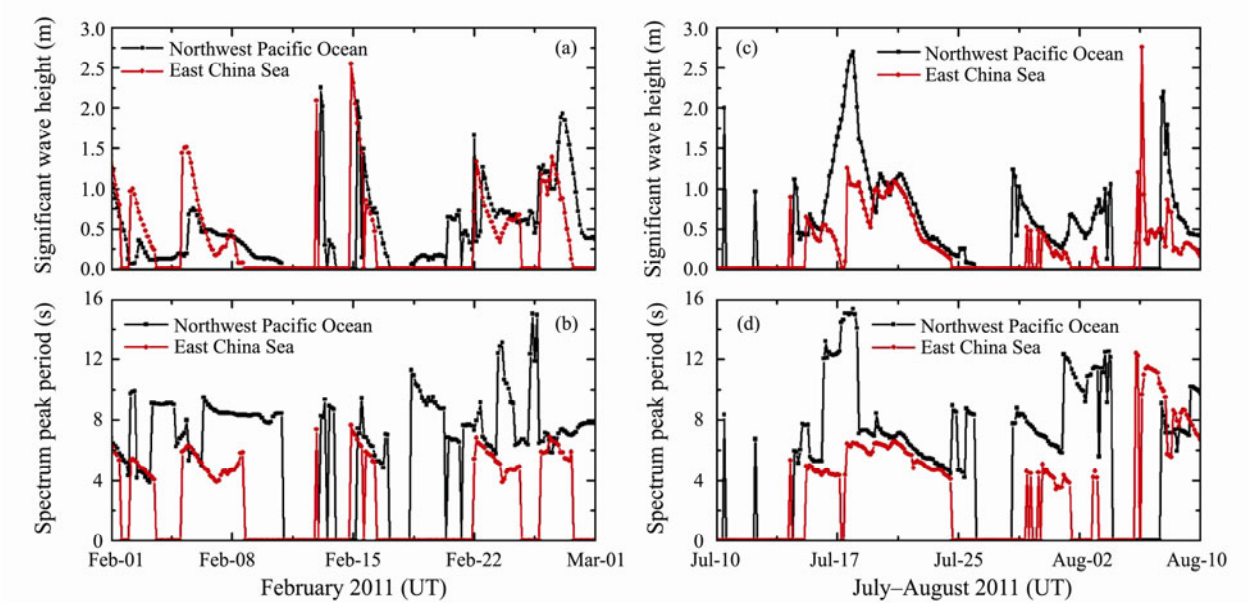

Fig.10 Calculated parameters of swells using different spatial scales for non-typhoon and typhoon scenarios. (a) and (b) are for non-typhoon scenarios and (c) and (d) are for typhoon scenarios.

The proportion of each swell state and corresponding range at P-point are calculated for the whole year of 2011; results are listed in Tables 3 and 4 for non-typhoon and typhoon scenarios, respectively. During non-typhoon scenarios, it can be seen that swells generated by the local wind account for the largest proportion (38%). However, swells originating from the adjacent sea occupy the largest proportion (43%) during typhoon scenarios. Both scenarios present a common state, in which significant wave heights and spectrum peak periods of swells generated by local wind are lower than those generated from the adjacent sea or from both areas.

To understand the variation between different years, a statistical analysis of results simulated within the East China Sea during 2010–2014 is made in this paper. The composition of swell at P-point in 2010–2014 is presented in Table 5, where it can be seen that for 6 months of each year, swells at P-point are those generated by the local wind field and from the adjacent sea. For around 25%–30% of the years, swells at P-point are only propagated from the adjacent sea, and swells at P-point are only generated by the local wind field for a small percentage

of the years. During the rest of the years there is no swell at P-point. in addition, there are only small differences in the composition of swells between different years, which means swell evolution trend is consistent.

Table 3 Statistics for four swell states during non-typhoon scenarios in 2011 at P-point

Swell state	Proportion	Range of characteristic parameter variation	
		SWH (m)	SPP (s)
Originates from adjacent sea	21%	0.06–2.55	4.5–15.0
Generated by local wind	38%	0.07–1.53	4.0–10.0
From both areas	29%	0.08–2.08	5.0–13.0
No swell	12%	–	–

Table 4 Statistics of four swell states during typhoon scenarios in 2011 at P-point

Swell state	Proportion	Range of characteristic parameter variation	
		SWH (m)	SPP (s)
Originates from adjacent sea	28%	0.06–2.03	5.0–15.0
Generated by local wind	13%	0.21–1.15	4.5–8.0
From both areas	43%	0.26–2.70	5.0–15.5
No swell	16%	–	–

Table 5 Composition of swell in East China Sea in 2010–2014

Composition of Swell	Proportion					
	2010	2011	2012	2013	2014	average
Originate from adjacent sea	34%	36%	25%	23%	22%	28%
Generated by local wind	5%	3%	4%	4%	5%	4%
Composition of both the above	39%	37%	49%	49%	55%	46%
No swell	22%	24%	22%	24%	18%	22%

4 Conclusions and Discussion

Using the WAVEWATCH III numerical model and basic data obtained from Etopo1 and CCMP, the wave fields of the North West Pacific, particularly the East China Sea, were simulated from 2010 to 2014. After separating swell and wind sea from mixed waves, the spatial and temporal distribution of swells and their mechanisms in the East China Sea were investigated. The significant wave heights of swells in the East China Sea are mainly distributed in the 0.1–2.5 m range, the interval with the highest frequency of occurrence is 0.1–0.5 m, and the proportion of occurrence is approximately 50%. The spectrum peak periods of swells are mainly distributed in the 4–15 s range, the interval with the highest frequency of occurrence is 9–15 s, and the proportion of occurrence approximately 25%. In terms of spatial distribution, swells increase gradually from offshore to the deep sea and increase gradually from the north to the south. Furthermore, the values of swells in the sea outside the Ryukyu chain are significantly greater than those in the area within the Ryukyu chain. There is a high similarity in the spatial distribution of swells in different years.

Swells in the East China Sea are affected by the local wind but swells also originate from other adjacent sea areas. From a compositional analysis of influential factors under different meteorological conditions, it is evident that during the non-typhoon scenarios, swells generated by local winds account for the largest proportion (approximately 38% of the simulation time zone). During the typhoon scenarios, swells originating from the adjacent sea account for the largest proportion (approximately 43% of the simulation time zone). From a composition analysis of influential factors within one year, it is determined that swells in the East China Sea are composed of those generated by the local wind field and from the adjacent sea for approximately 6 months of every year. For approximately 25%–30% of each year, swells in the East China Sea propagate only from the adjacent sea. However, swells in the East China Sea are only generated by the local wind field for a small percentage of time during each year. Therefore, it is evident that swells are common phenomena and are present for more than 9 months of every year; therefore further research on this topic would be meaningful.

Acknowledgements

This research work is funded by the National Natural Science Fundation of China (Nos. 51579091, 51379071, and 51137002), the National Science Fund for Distinguished Young Scholars (No. 51425901), the Qing Lan Project of Jiangsu Province, the Basic Research Fund from State Key Laboratory of Hydrology-Water Resources and Hydraulic Engineering, Hohai University (Nos. 20145027512 and 20145028412), the Short-term Research Visits project supported by Disaster Prevention Research Institute of Kyoto University (No. 27S-02), and the Fundamental Research Funds for the Central Universities of Hohai University (No. 2016B05214).

Reference

Amante, C., and Eakins, B. W., 2009. ETOPO1 1 Arc-Minute Global Relief Model: Procedures, data sources and analysis.

Psychologist, **16** (3): 20-25.

Hanson, J. L., and Phillips, O. M., 2001. Automated analysis of ocean surface directional wave spectra. *Journal of Atmospheric & oceanic Technology*, **18** (2): 277-293.

Hanson, J. L., Tracy, B. A., Tolman, H. L., and Scott, R. D., 2009. Pacific hindcast performance of three numerical wave models. *Journal of Atmospheric & Oceanic Technology*, **26** (26): 1614-1633.

Hemer, M. A., Fan, Y., Mori, N., Semedo, A., and Wang, X. L., 2013. Projected changes in wave climate from a multi-model ensemble. *Nature Climate Change*, **3** (5): 471-476, DOI: 10.1038/nclimate1791.

Liu, Z. H., Zheng, C. W., Zhuang, H., Jing, L. I., and Yao, X. F., 2011. Long-term trend and special characteristics of sea surface wind speed in the northwest Pacific Ocean during the last 22 years. *Ocean Technology*, **2**: 127-130.

Milliff, R. F., Morzel, J., Chelton, D. B., and Freilich, M. H., 2004. Wind stress curl and wind stress divergence biases from rain effects on QSCAT surface wind retrievals. *Journal of Atmospheric & Oceanic Technology*, **21** (8): 1216-1231.

Munk, W. H., and Snodgrass, F. E., 1957. Measurements of southern swell at Guadalupe Island. *Deep Sea Research*, **4** (4): 272-286.

Myers, V. A., 1954. *Characteristics of United States Hurricanes Pertinent to Levee Design for Lake Okechobeem, Florida*. Government Printing Office, **2**: 1-106.

Pei, Y., Tao, A. F., Zhang, Y. F., Li, H., and Yan, J., 2016. The generation mechanisms of low-frequency swell in the E3 sea area of the East China Sea. *Transaction of Oceanology and Limnology*, **1** (1): 17-24 (in Chinese).

Shimura, T., Mori, N., and Hemer, M. A., 2016. Variability and future decreases in winter wave heights in the Western North Pacific. *Geophysical Research Letters*, **43** (6): 2716-2722, DOI: 10.1002/2016GL067924.

Shimura, T., Mori, N., and Mase, H., 2013. Ocean waves and teleconnection patterns in the Northern Hemisphere. *Journal of Climate, American Meteorological Society*, **26**: 8654-8670.

Tao, A. F., Peng, J., Zheng, J. H., Su, Q., and Wu, Y. Q., 2014. The occurrence probabilities of rogue waves in random wave field. *Proceedings of 7th Chinese-German Joint Symposium on Hydraulic and Ocean Engineering*. Hannover, Germany.

Tolman, H. L., 2009. User manual and system documentation of WAVEWATCH III version 3.14. *Technical Note*, 166pp.

Tracy, B., Devaliere, E., Hanson, J., Nicolini, T., and Tolman, H., 2007. Wind sea and swell delineation for numerical wave modeling. In: *Proceedings of the 10th International Workshop on Hindcasting and Forecasting*. Oahu, USA.

Wang, Y., Tao, A. F., Zheng, J. H., Doong, D. J., Fan, J., and Peng, J., 2014. A preliminary investigation of rogue waves off the Jiangsu coast, China. *Natural Hazards & Earth System Sciences*, **14** (9): 2521-2527.

Ying, M., Zhang, W., Yu, H., Feng, J., and Fan, Y., 2014. An overview of the China Meteorological Administration tropical cyclone database. *Journal of Atmospheric & Oceanic Technology*, **31** (2): 287-301.

Zhang, R. C., Kawamura, H., and Toba, Y., 1988. Propagation characteristics of swell incoming from the deep ocean into the seas east of China. *Progress in Oceanography*, **21** (88): 441-455.

(Edited by Xie Jun)